Instantaneous GNSS-based Kinematic Relative Positioning and Attitude Determination using Multi-Antenna Configurations

P.J. Buist[1*], P.J.G. Teunissen[1,2], G. Giorgi[1], S. Verhagen[1]

[1] DEOS, Delft University of Technology, The Netherlands

(Tel:+31 15 278 2713, E-mail: P.J.Buist@TUDelft.nl)

[2] Spatial Sciences, Curtin University of Technology, Australia

Abstract: GNSS carrier phase observations can be applied for precise relative positioning. If three or more antennas are placed on a single platform we can also use these observations to determine the attitude of the platform. Currently, we are developing a method to rigorously integrate these two problems such that the attitude solution can be used to enhance relative positioning between several platforms. The basic theory for a three- and four-antenna configuration, situated at two platforms with at most two antennas on a single platform was developed and published in previous publications. In this contribution we will extend the method to be applicable with more antennas. We will show the theoretical improvement achievable as a function of the number of antennas on each platform. The method will be tested using simulated data. Furthermore, we will test the method using data collected in a dedicated field experiment of a more challenging application where the unconstrained baseline between the platforms will vary over a distance of a few kilometers. This contribution will show that the new method enhances especially the ambiguity resolution on the unconstrained baselines between platforms, both in terms of empirical success rate for ambiguity fixing and availability of a fixed baseline solution for the unconstrained baseline between the platforms.

Keywords: GNSS, Relative Positioning, Attitude Determination, LAMBDA, Ambiguity Resolution

1 INTRODUCTION

GNSS carrier phase observations can be applied for precise relative positioning. If three or more antennas are placed on a single platform we can also use these observations to determine the orientation (i.e. the attitude) of the platform. Traditionally, the attitude determination and relative positioning problems have been treated separately. Currently, we are developing a method to rigorously integrate these two problems such that the attitude solution can be used to enhance relative positioning. This paper introduces a method for multi-antenna ambiguity resolution for constrained and unconstrained baselines and describes the method mathematically. Unconstrained baselines are baselines for which a-priori information about the length is not available and constrained baselines are baselines for which the length is known and constant.

2 MODELLING

2.1 Model for unconstrained baselines

Most GNSS receivers make use of two types of observations: pseudo range and carrier phase. The pseudo range observations typically have an accuracy of decimeters, whereas carrier phase observations have accuracies up to millimeter level. The double difference observation equations can be written for a single baseline as a system of linearized observation equations [1]:

$$E(y) = Aa + Bb, \quad D(y) = Q_y \tag{1}$$

Where E is the mean or the expected value and D is the variance or dispersion of y. y is the vector of observed minus estimated double difference carrier phases and/or code observations of the order m, a is the unknown vector of ambiguities of the order n expressed in cycles rather than range to maintain their integer character, b is the baseline

vector, which is unknown for relative navigation applications but for which the length in attitude determination is generally known, B is the geometry matrix containing normalized line-of-sight vectors, A is a design matrix that links the data vector to the unknown vector a. In this paper the assumption is made that the antennas are close to each other and thus atmospheric affects can be neglected. The variance matrix of y is given by the positive definite matrix Q_y which is assumed to be known. As explained in [1], the least squares solution of the linear system of observation equations as introduced in Eq. (1) is obtained, using $\|..\|^2_{Q_y} = (..)^T Q_y^{-1}(..)$, from:

$$\min_{a\in\mathbb{Z}^n, b\in\mathbb{R}^3} \|y - Aa - Bb\|^2_{Q_y} \tag{2}$$

The variance-covariance (or v-c) matrix of the float solution $\hat{a}$ and $\hat{b}$, i.e. the solution of Eq. 2 obtained while disregarding the integer constraint on the ambiguities, is denoted as:

$$\left[(A,B)^T Q_y^{-1}(A,B)\right]^{-1} = \begin{bmatrix} Q_{\hat{a}} & Q_{\hat{a}\hat{b}} \\ Q_{\hat{b}\hat{a}} & Q_{\hat{b}} \end{bmatrix} \tag{3}$$

and for $\hat{b}(a)$, the least squares solution for b assuming that a is known, as $Q_{\hat{b}(a)} = Q_{\hat{b}} - Q_{\hat{b}\hat{a}} Q_{\hat{a}}^{-1} Q_{\hat{a}\hat{b}}$. The integer solution of this system can be obtained by applying the standard LAMBDA method [2][3][4].

2.2 Model for constrained baselines

For applications for which some of the baseline lengths are known and constant, as for example GNSS-based attitude determination, we can exploit the so-called baseline constrained model. Then the baseline constrained integer ambiguity resolution can make use of the standard GNSS model by adding the length constraint of the baseline $||b||_{I_3} = l$, where l is known. The least squares criterion for this problem reads

$$\min_{a\in\mathbb{Z}^n, b\in\mathbb{R}^3, ||b||_{I_3}=l} \|y - Aa - Bb\|^2_{Q_y} \tag{4}$$

This least squares problem is coined a Quadratically Constrained Integer Least Squares (QC-ILS) problem in [5]. The solution can be obtained with the baseline constrained LAMBDA method which is described in [6][7][8][9].

3 BASELINE CONSTRAINED MULTI-ANTENNA AMBIGUITY RESOLUTION

Precise relative positioning of two moving platforms usually requires dual-frequency phase data, whereas - due to the baseline length constraints - single-frequency phase data may suffice for the precise determination of platform attitudes [6][8][10]. These two GNSS problems, relative positioning and attitude determination, are usually treated separately and independent from one another. In this contribution, however, we will combine the two problems and apply a single processing strategy for solving them. As such, the problem becomes a multi-antenna ambiguity resolution problem of which some of the baseline lengths are constrained. First we will introduce a multi antenna configuration on two separate platforms. The basic theory for a three- and four-antenna configuration, situated at two platforms with at most two antennas on a single platform was developed in [11] and [12]. In these publications the performance of the method was also confirmed with simulated data and a simple field experiment utilizing three antennas on a single platform. In this contribution we will extend the method to be applicable with more antennas. We will show the theoretical improvement achievable as a function of the number of antennas on each platform. This solution for individual constrained baselines will always be suboptimal as not all information available is applied (e.g. the relative orientation of the baselines), and this limitation can be overcome by the multivariate constrained LAMBDA method described in [13]. However we will use the solution for individual baselines as a first step to prove the concept of the integrated approach.

3.1 Multi-Baseline Setup

As is shown in Fig. 1, in our multi-antenna configuration the number of antennas at a single platform is $N+1$ and the number of independent baselines is therefore N. Hence the number of baselines on a platform plus the unconstrained baseline to the other platform is again $N+1$. The first constrained baseline on platform 1 is called baseline b_1 and the last baseline b_N. In order to distinguish between antennas and baselines at different platforms we introduce a superscript indicating the platform, e.g. the first constrained baseline on platform 1 is written as b_1^1 in Fig. 1. The unconstrained baseline connecting the two platforms is then written as b^{12}, which is equal to $-b^{21}$ as indicated in Fig. 1. For compactness in this theoretical discussion the antennas are assumed to be sufficiently close, so that the relative antenna-satellite geometry may be considered the same for all antennas, so that the design matrices A and B and the variance-covariance matrix Q_y are assumed to be identical. In our software implementation, the design matrices are only assumed to be identical if they apply to antennas at the same platform. To describe the dispersion of the observations at all baselines we make use of $P \otimes Q_y$, where $\otimes$ is the the Kronecker symbol and matrix P takes care of the correlation that follows from the fact that the baselines have one antenna in common. For a discussion on matrix P, we refer to [11][12]. In this section we will apply an $(N+1)\times(N+1)$ tridiagonal matrix $P = \begin{bmatrix} 1 & -\frac{1}{2} & 0 & \dots & 0 \\ -\frac{1}{2} & 1 & -\frac{1}{2} & & \vdots \\ 0 & -\frac{1}{2} & 1 & \ddots & 0 \\ \vdots & & \ddots & \ddots & -\frac{1}{2} \\ 0 & \dots & 0 & -\frac{1}{2} & 1 \end{bmatrix}$.

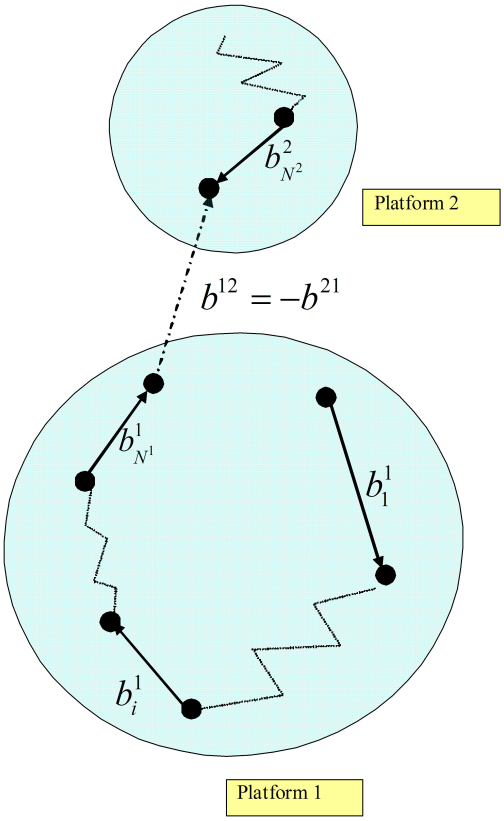

Fig. 1: Definition of the multi antenna configuration on two platforms

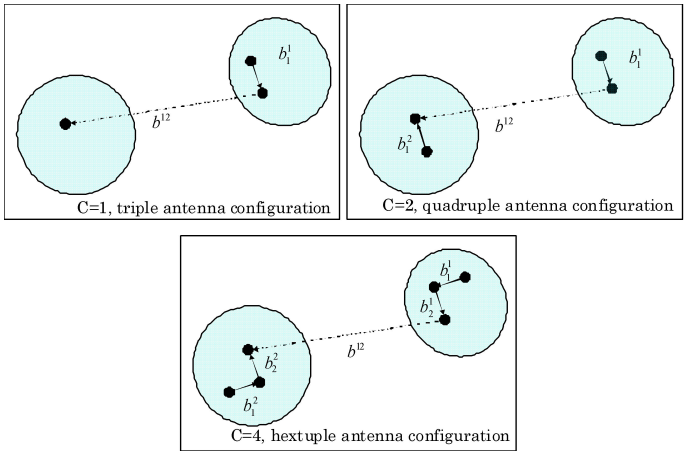

Fig. 2: Definition of two platforms and C antenna configuration

3.2 Model for an $N+1$ Antenna Configuration

In order to obtain the unknown parameters we need to solve the following minimization problem for a single platform with N constrained baselines, and a single unconstrained baseline to an antenna at another platform. The problem is subject to $||b_i^1|| = l_i^1$ and $a = (\cup_i a_i^1, a^{12})$ with $i = 1, \ldots, N^1$. In [11][12], it was demonstrated that for this model the float solutions for each baseline are solely determined by the double difference observation vector of the corresponding baseline and therefore the problem becomes:

$$\min_{a\in\mathbb{Z}^n} \left\| \begin{matrix} y_1^1 - Aa_1^1 - Bb_1^1 \\ \vdots \\ y_{N^1}^1 - Aa_{N^1}^1 - Bb_{N^1}^1 \\ y^{12} - Aa^{12} - Bb^{12} \end{matrix} \right\|^2_{P\otimes Q_y} = \left\| \begin{matrix} \hat{e}_1^1 \\ \vdots \\ \hat{e}_{N^1}^1 \\ \hat{e}^{12} \end{matrix} \right\|^2_{P\otimes Q_y} + \min_{a\in\mathbb{Z}^n} \left(\left\| \begin{matrix} \hat{a}_1^1 - a_1^1 \\ \vdots \\ \hat{a}_{N^1}^1 - a_{N^1}^1 \\ \hat{a}^{12} - a^{12} \end{matrix} \right\|^2_{P\otimes Q_{\hat{a}}} + \left\| \begin{matrix} \hat{b}_1^1(a_1^1) - b_1^1 \\ \vdots \\ \hat{b}_{N^1}^1(a_{N^1}^1) - b_{N^1}^1 \\ \hat{b}^{12}(a^{12}) - b^{12} \end{matrix} \right\|^2_{P\otimes Q_{\hat{b}(a)}} \right) \tag{5}$$

where $\hat{e} = y - A\hat{a} - B\hat{b}$ is the least squares residual of the float solution $\hat{a}, \hat{b}$.

Since there is no length constraint on b^{12}, it is possible to find a solution such that $\hat{b}^{12}(a^{12}) - b^{12} = 0$. Therefore this term can be omitted from the minimization problem. The last term of Eq. 5 can be decomposed as:

$$\left\| \begin{matrix} \hat{b}_1^1(a_1^1) - b_1^1 \\ \vdots \\ \hat{b}_{N^1}^1(a_{N^1}^1) - b_{N^1}^1 \\ \hat{b}^{12}(a^{12}) - b^{12} \end{matrix} \right\|^2_{P\otimes Q_{\hat{b}(a)}} = \left\|\hat{b}_1^1(a_1^1) - b_1^1\right\|^2_{Q_{\hat{b}(a)}} + \sum_{i=2}^{N^1} \left\|\hat{b}_i^1(a_i^1, b_I^1) - b_i^1\right\|^2_{X_i^1 Q_{\hat{b}(a)}} + \left\|\hat{b}^{12}(a^{12}, b_{N^1}^1, \ldots, b_1^1) - b^{12}\right\|^2_{X_{N^1+1}^1 Q_{\hat{b}(a)}} \tag{6}$$

with $\hat{b}_i^1(a_i^1, b_I^1)$ is the ith baseline conditioned on the ambiguity a_i and the previous baselines $b_I^1 = \cup_{j=1}^{i-1} b_j^1$.

With the constraint on both the baselines b_1^1 and the ambiguities, the conditional solution of the baseline b_2^1 becomes:

$$\hat{b}_2^1(a_2^1, b_1^1) = \hat{b}_2^1(a_2^1) + \frac{1}{2}\left(\hat{b}_1^1(a_1^1) - b_1^1\right) \tag{7}$$

With the constraint on the baselines b_1^1, b_2^1 and the ambiguities, the conditional solution of the baseline b_3^1 becomes:

$$\hat{b}_3^1(a_3^1, b_2^1, b_1^1) = \hat{b}_3^1(a_3^1) + \\ + \frac{2}{3}\left(\hat{b}_2^1(a_2^1) - b_2^1\right) + \frac{1}{3}\left(\hat{b}_1^1(a_1^1) - b_1^1\right) \tag{8}$$

and consistently for $\hat{b}^{12}(a^{12}, b_{N^1}^1, \ldots, b_1^1)$:

$$\hat{b}^{12}(a^{12}, b_{N^1}^1, \ldots, b_1^1) = \\ \hat{b}^{12}(a^{12}) + \frac{N^1}{N^1+1}\left(\hat{b}_{N^1}^1(a_{N^1}^1) - b_{N^1}^1\right) + \\ + \ldots + \frac{2}{N^1+1}\left(\hat{b}_2^1(a_2^1) - b_2^1\right) + \frac{1}{N^1+1}\left(\hat{b}_1^1(a_1^1) - b_1^1\right) \tag{9}$$

Using the relations we have found we can write the scaling factor X for the v-c matrix for the i-th baseline as:

$$\begin{aligned} &X_1^1 = 1 \\ &\text{For } i = 2, \ldots, N^1 + 1 = C + 1 \\ &\quad X_i^1 = 1 - \frac{1}{4X_{i-1}^1} \end{aligned} \tag{10}$$

where C indicates the number of constrained baselines in the configuration as will be explained later.
The integer least squares solution becomes for this N^1 constrained and one unconstrained baseline configuration:

$$\begin{bmatrix} \check{a}_1^1 \\ \check{a}_2^1 \\ \vdots \\ \check{a}_{N^1}^1 \\ \check{a}^{12} \end{bmatrix} = \arg\min_{a \in \mathbb{Z}^n} \left(\left\| \hat{a}_1^1 - a_1^1 \right\|_{Q_{\hat{a}}}^2 + \right. \\ + \left\| \hat{b}_1^1(a_1^1) - \check{b}_1^1(a_1^1) \right\|_{Q_{\hat{b}(a)}}^2 + \sum_{i=2}^{N^1} \left(\left\| \hat{a}_i^1(a_I^1) - a_i^1 \right\|_{X_i^1 Q_{\hat{a}}}^2 + \right. \\ \left. + \left\| \hat{b}_i^1(a_i^1, b_I^1) - \check{b}_i^1(a_i^1, b_I^1) \right\|_{X_i^1 Q_{\hat{b}(a)}}^2 \right) + \\ \left. + \left\| \hat{a}^{12}(a_{N^1}^1, \ldots, a_1^1) - a^{12} \right\|_{X_{N^1+1}^1 Q_{\hat{a}}}^2 \right) \tag{11}$$

for which

$$\left\| \hat{b}_1^1(a_1^1) - \check{b}_1^1(a_1^1) \right\|_{Q_{\hat{b}(a)}}^2 + \\ \sum_{i=2}^{N^1} \left\| \hat{b}_i^1(a_i^1, b_I^1) - \check{b}_i^1(a_i^1, b_I^1) \right\|_{X_i^1 Q_{\hat{b}(a)}}^2 = \\ \arg\min \left(\left\| \hat{b}_1^1(a_1^1) - b_1^1 \right\|_{Q_{\hat{b}(a)}}^2 + \right. \\ \left. + \sum_{i=2}^{N^1} \left\| \hat{b}_i^1(a_i^1, b_I^1) - b_i^1 \right\|_{X_i^1 Q_{\hat{b}(a)}}^2 \right)$$

is subject to $||b_i^1|| = l_i^1$ with $i = 1, \ldots, N^1$ and $(a_I^1) = \cup_{j=1}^{i-1} a_j^1$.
An approximation of the integer least squares solution can be obtained by solving the baselines sequentially where the solution of baseline i is applied on the next, as if the correlation between baselines would be absent [12]. The result is a vectorial bootstrapping approach in which we first solve the ambiguity on the constrained baselines and finally apply the found ambiguity vector in the solution of the unconstrained baseline. From Eq. 11 it is clear that the reduction on the dispersion (i.e. the scaling factor) on the baseline and ambiguity vectors is the same. This relationship is consistent with the scaling factors obtained in [12] where it was shown that in a triple antenna configuration with a constrained baseline at one side of the unconstrained baseline (i.e. the C=1 configuration in Fig. 2), the dispersion of ambiguity vector is reduced from $Q_{\hat{a}}$ to $\frac{3}{4}Q_{\hat{a}}$, or with three antennas on one platforms and one at the other to $\frac{2}{3}Q_{\hat{a}}$. The first row in Table 1 shows this scaling factor of $Q_{\hat{a}}$ for a platform with up to 11 antennas (i.e. 10 baselines). The same relation is also valid for the ith constrained baseline for an antenna configuration on a single platform. Hence we expect the success rate for the ambiguity resolution on ith constrained baseline to increase due to the smaller $Q_{\hat{a}}$ compared with the $i-1$ constrained baseline.
A similar general formula can be derived if the unconstrained baseline between the two platforms is constrained by constrained baselines at both sides. It was demonstrated in [12] that for the quadruple antenna configuration with a constrained baseline, b_1^1 and b_1^2 respectively, on both sides of the unconstrained baseline b^{12} between the two platforms (i.e. the C=2 configuration in Fig. 2), we can write:

$$\left\| \begin{matrix} \hat{b}_1^1(a_1^1) - b_1^1 \\ \hat{b}_1^2(a_1^2) - b_1^2 \\ \hat{b}^{12}(a^{12}) - b^{12} \end{matrix} \right\|_{P \otimes Q_{\hat{b}(a)}}^2 = \left\| \hat{b}_1^1(a_1^1) - b_1^1 \right\|_{Q_{\hat{b}(a)}}^2 + \\ + \left\| \hat{b}_1^2(a_1^2) - b_1^2 \right\|_{Q_{\hat{b}(a)}}^2 + \left\| \hat{b}^{12}(a^{12}, b_1^1, b_1^2) - b^{12} \right\|_{\frac{1}{2}Q_{\hat{b}(a)}}^2 \tag{12}$$

With the constraint on the baselines b_1^1,b_1^2 and the ambiguities, the conditional solution of the baseline b^{12} becomes:

$$\hat{b}^{12}(a^{12}, b_1^1, b_1^2) = \hat{b}^{12}(a^{12}) + \\ + \frac{1}{2}\left(\hat{b}_1^1(a_1^1) - b_1^1\right) + \frac{1}{2}\left(\hat{b}_1^2(a_1^2) - b_1^2\right) \tag{13}$$

In the model described in section 3.1, the observations collected at the two platforms are uncorrelated, except for the two antennas on the unconstrained baseline connecting the two platforms. In this contribution we will solve the set of constrained baselines at each platform separately.
Now we can also extend this theory to a general model for a multi-antenna configuration at both platforms with N^1 con-

strained baselines $b_1^1, \ldots, b_{N^1}^1$ at the first platform, N^2 constrained baselines $b_1^2, \ldots, b_{N^2}^2$ at the other platform and the unconstrained baseline between both platforms defined as $b^{12} = -b^{21}$. We can write:

$$\left\| \begin{array}{c} \hat{b}_1^1(a_{12}^1) - b_1^1 \\ \vdots \\ \hat{b}_{N^1}^1(a_{N^1}^1) - b_{N^1}^1 \\ \hat{b}_1^2(a_1^2) - b_1^2 \\ \vdots \\ \hat{b}_{N^2}^2(a_{N^2}^2) - b_{N^2}^2 \\ \hat{b}^{12}(a^{12}) - b^{12} \end{array} \right\|^2_{P \otimes Q_{\hat{b}(a)}} =$$

$$\left\|\hat{b}_1^1(a_1^1) - b_1^1\right\|^2_{Q_{\hat{b}(a)}} + \sum_{i=2}^{N^1} \left\|\hat{b}_i^1(a_i^1, b_I^1) - b_i^1\right\|^2_{X_i^1 Q_{\hat{b}(a)}} +$$

$$+ \left\|\hat{b}_2^2(a_2^2) - b_2^2\right\|^2_{Q_{\hat{b}(a)}} + \sum_{i=2}^{N^2} \left\|\hat{b}_i^2(a_i^2, b_I^2) - b_i^2\right\|^2_{X_i^2 Q_{\hat{b}(a)}} +$$

$$+ \left\|\hat{b}^{12}(a^{12}, b_{N_1}^1, b_{N_2}^2, \ldots, b_1^1, b_1^2) - b^{12}\right\|^2_{(X_{N^1 N^2}^{12}) Q_{\hat{b}(a)}} \quad (14)$$

The scaling factor $X_{N^1 N^2}^{12}$ for an unconstrained baseline connected to N^1 constrained baselines at a platform at one side and N^2 constrained baselines at a platform at the other side can be written as:

$$\begin{aligned} & X_1^1 = 1, X_1^2 = 1 \\ & \text{For i=2 till } N^1 \\ & \quad X_i^1 = 1 - \frac{1}{4X_{i-1}^1} \\ & \text{For i=2 till } N^2 \\ & \quad X_i^2 = 1 - \frac{1}{4X_{i-1}^2} \\ & X_{N^1 N^2}^{12} = 1 - X_{N^1}^1 - X_{N^2}^2 \\ & C = N^1 + N^2 \end{aligned} \quad (15)$$

The second row in Table 1 shows the scaling factor of $Q_{\hat{a}}$ for the unconstrained baseline between two platforms each with up to 11 antennas. The relation is shown as function of baseline number at one side or at two sides of the unconstrained baseline in Fig. 3. As this figure shows with constraints on one side, the scaling factor approaches $\frac{1}{2}$, and with constraints on both sides this factor will go to a very small value. This means that the improvement is larger with constraints at both sides as the model becomes stronger. With the constraints on one side the model is weaker as the unconstrained baseline is now only constrained at one side and the other side is left free.

For some applications a platform will already have a number of antennas: for example 3 antennas are required, and 4 antennas are common, for platforms using GNSS for full attitude determination [14]. Therefore we will investigate the cases marked in Table 1 further in section 5. These cases are also shown in Fig. 2 as C=1, C=2 and C=4.

$\#C$	1	2	3	4	5	6	7	8	9	10
One side	3/4	2/3	5/8	3/5	7/12	4/7	9/16	5/9	11/20	6/11
$\#C$	2	4	6	8	10	12	14	16	18	20
Two side	1/2	1/3	1/4	1/5	1/6	1/7	1/8	1/9	1/10	1/11

Table 1: Scaling factor for the v-c matrix as a function of the number of constrained baselines, the grey color indicates cases that will be simulated in section 5.1

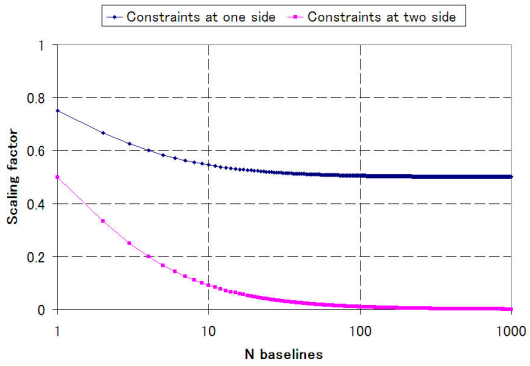

Fig. 3: Relationship between number of constrained baseline and the scaling factor for the v-c matrix

3.3 Discussion

The improvement for the precision of the v-c matrix in the multi-antenna configuration can be explained as follows. First we will discuss the symmetric case of having the same number of antennas $N + 1$ on each of the two platforms. If we start with the configuration $C = 0$, thus with 1 antenna on each platform, which gives 1 unconstrained baseline between the two platforms. The scaling factor for $Q_{\hat{a}}$ is then 1. Next we continue with 2 antennas on each platform (configuration $C = 2$) and we assume that the baseline lengths between antenna $1-2$ at each platform are known. Then the ambiguities at these baselines can be determined successfully and therefore baselines b_1^1 and b_1^2 can be determined very precisely (mm-range) and thus almost exactly. But this means that the position of antenna 1 can be considered the same as that of antenna 2 for both platforms. Hence, we now have observed the 'same' unconstrained baseline (namely b_1^{12} and b_2^{12} in Fig. 4) twice. Thus the variance of the baseline estimate will improve by a factor $1/2$. This explanation can be extended to a larger number of constrained baselines at each platform but also for the non-symmetric case with a different number of antennas at each platform. Of course for real applications, even for a very large number of baselines,

the scaling factor will not become zero as there are remaining biases and errors not included in our model (e.g. absolute positioning errors at both platforms, ionosphere, multipath, etc), but the improvement is evident. Another assumption is that we can solve the ambiguities on the constrained baselines with a success rate of close to 100% which seems feasible as was demonstrated in [6][8], especially if we include the geometry of the antenna placement [13].

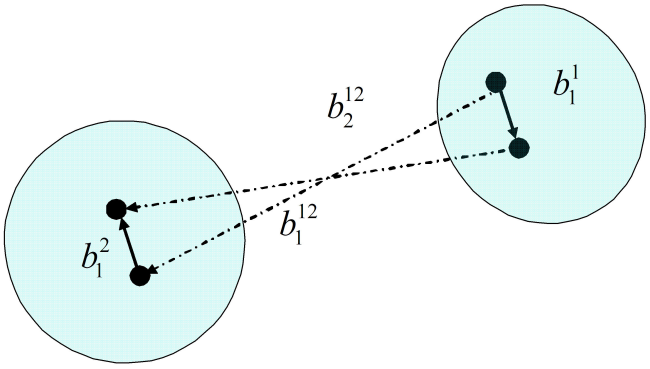

Fig. 4: Definition of two unconstrained baselines for the two platforms and C=2 antenna configuration

4 EXPERIMENT DESCRIPTION

4.1 Software Simulation Setup

Scenario	Triple, Quadruple and Hextuple antenna, orthogonal configuration
Frequency	L1
Number of Satellites	5 - 6 - 7 - 8
Undifferenced code noise σ_p $[cm]$	30 - 15 - 5
Undifferenced phase noise σ_ϕ $[mm]$	3 - 1
Baseline length $\|b_{ij}\| = l$	2.0 m
$\|b_{ij}\|$	150.0 m
Epochs simulated	10^5

Table 2: Simulation specification

In order to investigate the performance of the proposed integrated approach, we analyze as a first step the empirical success rates using simulated data. Table 2 summarizes the conditions of the simulations. Utilizing the VISUAL software [15], based on the location of the receivers and an actual GPS constellation, the design matrices of the model are calculated. Assuming different levels of noise on the undifferenced phase (from 1 mm to 3 mm) and undifferenced code (from 5 cm to 30 cm) data, a set of 10^5 data was generated; then each simulation was repeated for different number of satellites varying between 5 and 8.

4.2 Vessel Experimental Setup

For the demonstration with real data of the integrated approach described in section 3 we will use data for which the orientation of the baseline vectors at one of the platforms is relatively slowly changing. This data was collected onboard a vessel. The distance between the moving vessel and static reference station is between 2.5 and 4.5 km. Details about this experiment can be found in [16][8][10]. For this experiment three dual frequency GPS receivers, two geodetic grade (Leica SR530 and Ashtech Z12 connected to antenna $A1$ and $A2$ in Fig. 5 respectively) and one navigational type of receiver (NovAtel OEM3 connected to antenna $A3$ in Fig. 5) were utilized. These two antennas form a baseline of about 2.0 and 0.84 meter respectively. As the antennas are placed on their own mast, are using a choke-ring (Ashtech) or are survey grade (Leica AT502) and have a relatively free field-of-view, the impact of blocking and multipath on the observations is small. At the reference station, also three receivers where utilized with the configuration as shown in Fig. 6. At this side of the unconstrained baseline, always the Ashtech Z12 receiver with an Ashtech choke-ring with Dorne Margolin element is the master (G1), and Trimble 4700 and Novatel OEM3 with a NovAtel PinWheel 600 antennas are the auxiliary receivers (G2 and G3 respectively). The baseline vectors at the reference station have a length of 16.64 and 3.78 meter respectively.

As is well known, the low elevation satellite observations are in general less accurate due to for example multipath and unmodeled tropospheric delays, therefore we will apply a 15 degrees elevation mask for all observations.

The theoretical ambiguity success rate, i.e. probability of correct integer estimation, can be used to analyze the performance on the unconstrained baseline in the integrated approach and therefore is introduced in this section. As described in [17], a lower bound L_B of the probability of obtaining the correct integer ambiguity vector is:

$$P(\breve{a} = a) \geq L_B(Bootstrapped) \tag{16}$$

Important to note is that the lower bound for the ambiguity success rate are only valid for unconstrained baselines. The lower bound of the probability of obtaining the correct ambiguity vector can be used to analyze how much the success rate in theory could improve for the ambiguity estimator of the unconstrained baseline in the integrated approach compared to the standalone solution of the unconstrained baseline. Normally in a relative positioning algorithm, we make use of a heuristic minimum success rate. If the success rate is lower than this threshold no attempt is made to fix the ambiguities. Especially for single frequency we have to use a low threshold because otherwise almost never an attempt is made to resolve ambiguities in our experiment [10]. In this research, as we like to investigate the empirical success rate, we will not make use of such a threshold for ambiguity fixing. However we will analyze for how many epochs the theoretical success rate is higher than the threshold of 0.5

which was applied in [10].

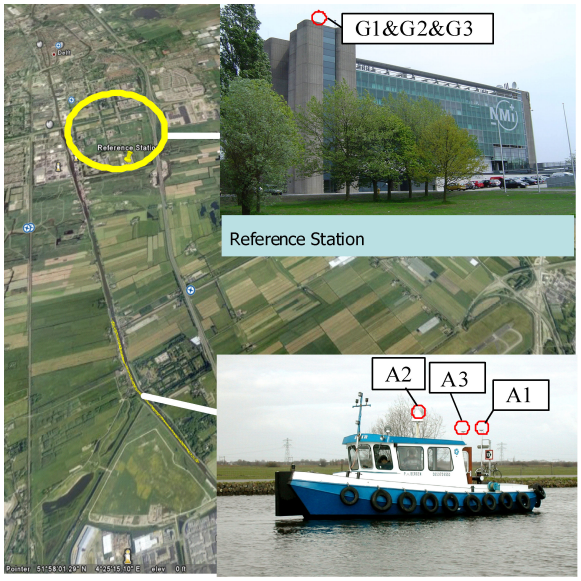

Fig. 5: Vessel Experiment

5 EXPERIMENTAL RESULTS

5.1 Software Simulations

In this section we will analyze the integrated approach for the antenna configurations in Fig. 2. We analyze the solution using one constrained baseline as in the triple antenna configuration ($C = 1$), two constrained baselines as in the quadruple ($C = 2$) and four as in the hextuple antenna configuration ($C = 4$). The results are presented in two tables. Table 3 and 4 contain empirical success rates as a function of the number of tracked satellites (N_{SV}) and the phase and code noise (σ_ϕ, σ_p). In Table 3 and 4, we analyze the success rate on individual baselines, both standalone and as part

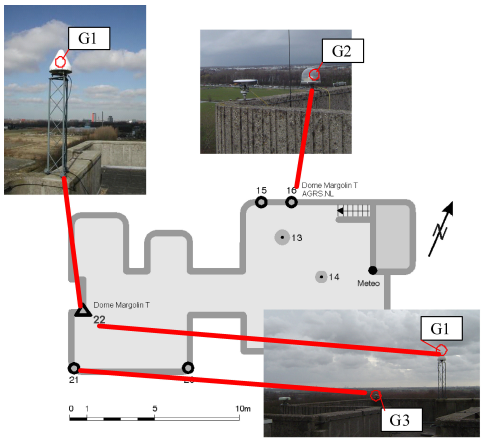

Fig. 6: Antenna definition at reference station for the Vessel Experiment

N_{SV}	$\#C$	σ_ϕ [mm]=3			σ_ϕ [mm]=1		
		σ_p [cm]			σ_p [cm]		
		30	15	5	30	15	5
	2	*First constrained baseline* $P(\check{a}_1^1 = a_1^1)$					
	4	*Second constrained baseline* $P(\check{a}_2^1 = a_2^1)$					
	2	0.72	0.89	1.00	0.97	1.00	1.00
5	4	0.77	0.92	1.00	0.99	1.00	1.00
	2	0.96	0.99	1.00	1.00	1.00	1.00
6	4	0.98	1.00	1.00	1.00	1.00	1.00
	2	0.99	1.00	1.00	1.00	1.00	1.00
7	4	1.00	1.00	1.00	1.00	1.00	1.00
	2	1.00	1.00	1.00	1.00	1.00	1.00
8	4	1.00	1.00	1.00	1.00	1.00	1.00

Table 3: Simulation results: single-frequency, single-epoch success rates for the constrained baseline b_1^1 using one constrained baseline ($C = 2$, i.e. two antennas) and on the second baseline b_2^1 in two constrained baseline ($C = 4$, i.e. three antennas) on a single platform

of the integrated solution.

For the unconstrained baseline we will analyze the standalone case, the case where one constrained baseline is utilized ($C = 1$), the case where two ($C = 2$) or four ($C = 4$) constrained baselines are utilized.

We investigated also the overall empirical success rate, which is the success rate on both baselines ($P(\check{a}_1^1 = a_1^1, \check{a}^{12} = a^{12})$) for the triple antenna configuration in a combined solution, ($P(\check{a}_1^1 = a_1^1, \check{a}_1^2 = a_1^2, \check{a}^{12} = a^{12})$) in a quadruple configuration, and the success rates ($P(\check{a}_1^1 = a_1^1, \ldots, \check{a}^{12} = a^{12})$) on all five baselines in the hectuple antenna configuration. So again the uncoupled and integrated approach using one, two or four constrained baseline(s) are considered. The results for overall success rate are mainly limited by the unconstrained baseline and therefore are almost the same as Table 4. The maximum difference is around 5% for the weaker models and therefore these results are not included in this publication.

In Table 4, the unconstrained baseline b^{12} is presented as standalone ($C = 0$) and as part of the the combined solution using a single constrained baseline ($C = 1$) and using two or four constrained baselines ($C = 2$ and $C = 4$). As expected, when comparing Table 3 and 4, the baseline constrained solution clearly provides much better results than the unconstrained solution. The differences in success rate are particularly pronounced when the strength of the underlying GNSS model becomes weaker (fewer satellites and/or higher measurement noise). According to Table 3 already 5 satellites and a phase standard deviation of 3 mm gives a higher than 70% success rate for the constrained solution. We observe that the success rate of the second constrained baseline in this table is always equal to or higher than that on the first baseline. This is expected from section 3.2, where it was demonstrated that the dispersion is reduced to $\frac{3}{4}$ of the original $Q_{\hat{a}}$

For the unconstrained baseline in Table 4 we observe that

N_{SV}	$\#C$	σ_ϕ $[mm]$=3			σ_ϕ $[mm]$=1		
		σ_p $[cm]$			σ_p $[cm]$		
		30	15	5	30	15	5
5	0	0.03	0.19	0.87	0.06	0.27	0.95
	1	0.04	0.26	0.93	0.09	0.36	0.98
	2	0.09	0.42	0.98	0.15	0.52	1.00
	4	0.09	0.51	0.99	0.23	0.69	1.00
6	0	0.25	0.67	0.97	0.49	0.87	1.00
	1	0.36	0.80	0.99	0.59	0.92	1.00
	2	0.55	0.92	1.00	0.74	0.97	1.00
	4	0.68	0.97	1.00	0.85	0.99	1.00
7	0	0.50	0.80	1.00	0.75	0.93	1.00
	1	0.61	0.89	1.00	0.81	0.97	1.00
	2	0.74	0.96	1.00	0.89	0.99	1.00
	4	0.85	0.99	1.00	0.95	1.00	1.00
8	0	0.86	0.95	1.00	1.00	1.00	1.00
	1	0.92	0.97	1.00	1.00	1.00	1.00
	2	0.97	0.99	1.00	1.00	1.00	1.00
	4	0.99	1.00	1.00	1.00	1.00	1.00

Table 4: Simulation results: single-frequency, single-epoch success rates for the unconstrained baseline using zero ($C = 0$), one ($C = 1$, i.e. triple antenna configuration), two ($C = 2$, i.e. quadruple antenna configuration) or four ($C = 4$, i.e. Hextuple antenna configuration) constrained baselines

the combined approach has a better performance than standalone. The improvement is between 0 and 13% using a single constrained baseline ($C = 1$), between 0 and 30% using two constrained baselines ($C = 2$) and between 0 and 43% using four constrained baselines ($C = 4$), with a larger improvement for weaker GNSS models.

Triple vs. Quadruple vs. Hextuple Antenna Configuration

The probability of obtaining the correct integer value increases as the precision of $\hat{a}$ improves. For the unconstrained baseline in the quadruple antenna configuration (case $C = 2$ in Table 4) we observe a higher success rate than for the same baseline in the triple antenna configuration (case $C = 1$ in Table 4), which is as expected as the variance-covariance matrix is scaled with $\frac{1}{2}$ and $\frac{3}{4}$ respectively of the original $Q_{\hat{a}}$ of the standalone solution. The unconstrained baseline in the hextuple antenna configuration is scaled with $\frac{1}{3}$. Therefore we can say that the larger number of constrained baselines in an antenna configuration results in a stronger model. Another important result is that the availability of an fixed solution for the unconstrained baseline will increase remarkably for the integrated approach compared with standalone. Normally only if the lower bound of the success rate is higher than a certain threshold an attempt will be made to fix the ambiguities. In Table 4, the cases are colored grey for which the standalone approach is below a threshold of 95%, but the integrated approach is higher than this threshold.

5.2 Vessel Experiment

An important difference between the field experiment and the simulated results in section 5.1 is that the phase and code noise levels for all receivers in the simulations are the same, whereas for the field experiment, as we make use of receivers from 4 different manufacturers which are physical located at different environments (vessel vs. reference station), the noise levels are different. This is a main challenge for our software design, but for most applications we expect that similar receivers will be utilized. Due to this difference in noise levels we can observe some interesting results as we will discuss in this section.

Fig. 7 shows the PDOP and number of locked satellites for all three receivers onboard the vessel during the experiment. During the whole experiment between 6 and 8 satellites are locked for all three receivers and PDOP is below 5. The estimated distance between the reference station and the vessel is shown in Fig. 8 and the attitude estimate for the vessel obtained as part of the integrated solution is shown in Fig. 9. We use the same approach as described in [18] to combine data from the two baselines into an attitude estimation. These two figures provide a good idea of the dynamics of our experiment. The baseline length varies between 2.5 and 4 kilometer. The bank and elevation angles remain fairly constant, but the maneuvers up and down the Schie river causes heading changes over 360 degrees.

The equation for the lower bound of the success rate of ambiguity resolution described in section 4.2 can also give us insight in the difference between the theoretical success rates of single frequency ambiguity resolution using the uncoupled and the integrated approach. Fig. 10 shows the theoretical minimum success rate, which is only valid for the unconstrained baseline, for each epoch using the actual user-GPS geometry for the uncoupled and integrated approach (C=4), where the integrated approach has a reduced dispersion of $\frac{1}{3}$ of the original $Q_{\hat{a}}$. These figures show that the success rate with the uncoupled approach is much lower than with the integrated approach. For the uncoupled approach often the minimum success rate is lower than the threshold described in section 4.2, which would result in a reduced number of epochs where an attempt is made to fix the ambiguities. From Table 5, it is also clear that due to the improved lower bound of the success rate, much more often an attempt is made to fix the ambiguities and therefore the integrated approach not only improves the empirical success rate, as will be discussed next, but also the availability of a solution.

Empirical ambiguity success rates of the vessel experiment are shown in Table 6 and 7. The standalone results are different from the results reported in [10], as in that publication only an attempt to resolve the ambiguities was made if the theoretical success rate was larger than the threshold of 0.5. In this research, for a fair comparison with the simulation

results in section 5.1, we will always try to resolve ambiguities.

In Table 6, the constrained baselines containing the geodetic grade receiver (G1 and G2, A1 and A2) have the highest success rate. The baselines containing the navigational receivers (G3 and A3) have a lower success rate, which is expected from the lower accuracy of the observations. If we compare the result for G1-G1 and A1-A2 with the simulated results shown in Table 3, we see that the increase in success rate is similar to the case with 7 satellites and a code noise of respectively 30 centimeter and carrier noise of 3 mm. For G2-G3 and A2-A3, the increase in success rate is similar to the case with 6 satellites and a code noise of respectively 30 centimeter and carrier noise of 3 mm. From Fig. 7, we know that the real number of satellites is higher than 6, namely 7 or 8, and therefore the noise values are higher on the observations than 30 cm and 3 mm for code and carrier respectively, or the assumption of normal distribution for the noise might not be valid (i.e. the observations contain code and or carrier multipath). As with the simulations, we observe that the success rate of the second constrained baseline in this table is always equal to or higher than that on the first baseline. This is expected from section 3.2, where it was demonstrated that the dispersion on the second baseline is reduced to $\frac{3}{4}$ of the original $Q_{\hat{a}}$.

Next we will analyze the unconstrained baseline using all three receivers onboard the vessel. As we use different receivers on the vessel side of the unconstrained baseline, the constrained baseline(s) at the vessel will also be used in different combinations. At the reference station we will only use data from the Ashtech receiver G1 as the reference station side of the unconstrained baseline. So on this side the order of the constrained baseline(s) is always the same. From [10], we know that the Ashtech receiver A2 has the best performance in combination with the same receiver at the reference station. We did not, as expected, observe influence of the baseline length, varying between 2.5 and 4.2 kilometers, on the success rate was. In Table 7, it is shown that, as expected, unconstrained baselines containing the geodetic grade receivers (A1 and A2) have a higher empirical success rate than the baselines containing the navigational receiver (A3). The increase in success rate for the unconstrained baselines in this field experiment is in line with our expectation from the simulation results presented in section 5.1. For example, the success rate for the unconstrained baseline between antenna A2 and the reference station is very similar to the case with 8 satellites and code and carrier noise of 30 cm and 3 mm in Table 4, and for the unconstrained baseline between A1 and the reference station is very similar to case of 7 satellites with code and carrier nose of 30 cm and 1 mm. The navigational type of receiver is not accurate enough to improve the empirical success rate on the unconstrained baseline between the reference station and antenna A1 and A2, and therefore this result is not included in the table. We observed a decrease in success rate of about 7% for the unconstrained baselines G1-A1 and G1-A2 for case C=4. This is also expected as in our approach the second baseline is bootstrapped from the solution for the first baseline. For a bootstrapped solution it is important to start with the most accurate solution and utilize this to improve the less accurate one. An opposite order might result in lower success rates for the more precise baseline in the integrated approach than, for example, standalone.

$\#C$	*Baseline between Reference Station and the Vessel*		
	G1-A1	G1-A2	G1-A3
0	4431	4775	3181
1	6336	6770	6404
2	9009	8660	8276
4	9303	8974	8436

Table 5: Vessel results: number of epoch for which the single-frequency, single-epoch theoretical success rates is larger than the threshold of 0.5 for the unconstrained baseline using zero ($C = 0$), one ($C = 1$, i.e. triple antenna configuration), two ($C = 2$, i.e. quadruple antenna configuration) or four ($C = 4$, i.e. Hextuple antenna configuration) constrained baselines

For the same reason we observe that the navigational receiver (A3) with corresponding higher noise levels for the observations, gains the most from the integrated approach. In the uncoupled approach this baseline has a success rate of 35%. If the Novatel receiver is supported with the constrained baseline to the Ashtech receiver connected to antenna A2 (configuration C=1), the success rate will go up to 62 %. Using a second constrained baseline at the other side of the unconstrained baseline between the reference station and the vessel will not help the solution much as the success rate will only increase 1%. This indicates that the navigational receiver onboard the vessel gains the most from the integrated approach. This is also expected from the theory and simulation results as this is the weakest model, caused by the lower accuracy of the observations and the local environment (c.q. blocking and multipath, a moving platform) of the receiver. Applying a second constrained baseline at both sides will result in a success rate of 73%.

6 CONCLUSIONS

In this paper we extended the method for the combination of both relative positioning and attitude determination for moving platforms, each having multi-antennas with known baseline lengths. The rigorous method makes use of all the information available (the integerness of the ambiguities,

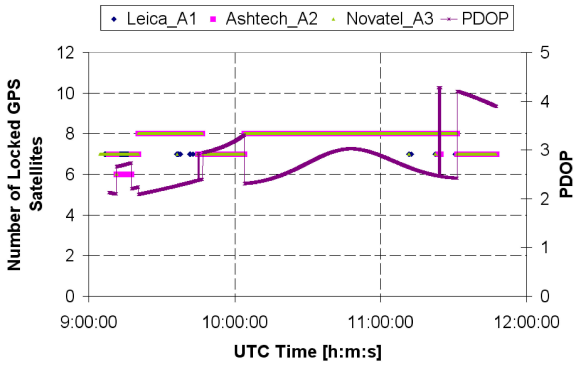

Fig. 7: Number of Locked satellites and PDOP for the receivers at the vessel

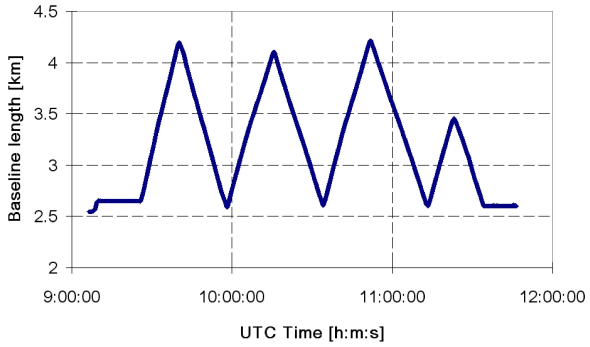

Fig. 8: Relative Navigation Result; baseline length between reference station and vessel

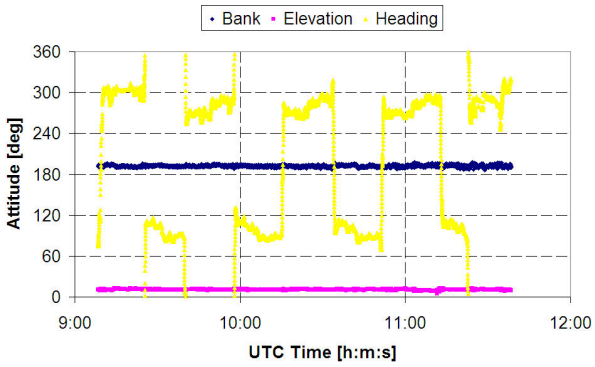

Fig. 9: Relative Navigation Result; Attitude estimate of the vessel

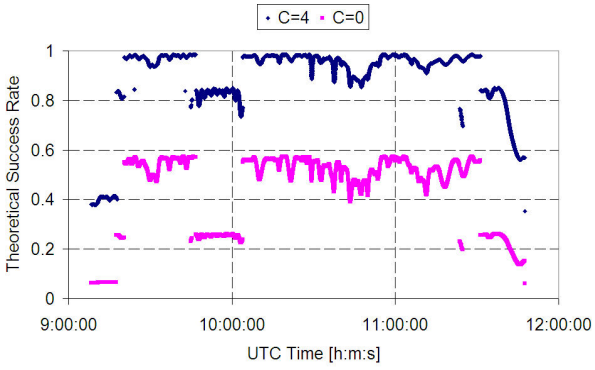

Fig. 10: Relative Navigation Result; Theoretical success rate for $C = 0$ and $C = 4$

$\#C$	*Reference Station*		*Vessel*	
	G1-G2	G2-G3	A1-A2	A2-A3
2	*First constrained baseline* $P(\tilde{a}_1^1 = a_1^1)$			
4	*Second constrained baseline* $P(\tilde{a}_2^1 = a_2^1)$			
2	0.99	0.96	1.00	0.94
4	1.00	0.97	1.00	0.95

Table 6: Vessel results: single-frequency, single-epoch success rates for the constrained baseline b_1^1 using one constrained baseline ($C = 1$, i.e. two antennas) and on the second baseline b_2^1 using two constrained baselines ($C = 2$, i.e. three antennas) on a single platform

$\#C$	*Baseline between Reference Station and the Vessel*		
	G1-A1	G1-A2	G1-A3
0	0.77	0.86	0.35
1	0.86	0.92	0.62
2	0.90	0.90	0.63
4	[1]	[1]	0.73

Table 7: Vessel results: single-frequency, single-epoch success rates for the unconstrained baseline using zero ($C = 0$), one ($C = 1$, i.e. triple antenna configuration), two ($C = 2$, i.e. quadruple antenna configuration) or four ($C = 4$, i.e. Hextuple antenna configuration) constrained baselines

[1] The navigational receivers (G3 and A3) are not accurate enough to enhance the results for the geodetic grade receivers (G1,G2,A1,A2), see text for more details

the relationship between the ambiguities on the different baselines and the known baseline length of the constrained baselines) to determine the relative position and orientation of a multi-antenna system with unconstrained and constrained baselines. The developed method improves both the availability and the success rate of the ambiguity resolution on the unconstrained baseline and the overall success rate of ambiguity resolution between a number of antennas. The basic theory for a three- and four-antenna configuration, situated at two platforms with at most two antennas on a single platform was developed and published in previous publications. In this contribution we extended the method to be applicable with more antennas. We showed the theoretical improvement achievable as a function of the number of antennas on each platform. This result was confirmed with simulated data and data collected in a field experiment.

ACKNOWLEDGMENTS

Peter Buist is supported by the MicroNed-MISAT framework. Professor Teunissen is the recipient of an Australian Research Council Federation Fellowship (project number FF0883188). The research of Sandra Verhagen is supported by the Dutch Technology Foundation STW, applied science division of NWO and the Technology Program of the Min-

istry of Economic Affairs. All this support is greatly acknowledged.

REFERENCES

[1] P J G Teunissen and A Kleusberg. GPS for Geodesy. *Springer, Berlin Heidelberg New York*, 1998.

[2] P J G Teunissen. Least Squares Estimation of the Integer GPS Ambiguities. *Invited lecture, Section IV Theory and Methodology, IAG General Meeting, Beijing*, 1993.

[3] P J G Teunissen. The Least-Squares Ambiguity Decorrelation Adjustment: a Method for Fast GPS Integer Ambiguity Estimation. *Journal of Geodesy*, 70:65–82, 1995.

[4] P J G Teunissen. An Optimality Property of the Integer Least-Squares Estimator. *Journal of Geodesy*, 73(11):587–593, 1999.

[5] P J G Teunissen. Integer Least Squares Theory for the GNSS Compass. *Journal of Geodesy, Springer, submitted*, 2009.

[6] C Park and P J G Teunissen. A New Carrier Phase Ambiguity Estimation for GNSS Attitude Determination Systems. *Proceedings of International GPS/GNSS Symposium, Tokyo*, 2003.

[7] P J G Teunissen. The LAMBDA Method for the GNSS Compass. *Artificial Satellites*, 41(3):89–103, 2006.

[8] P J Buist. The Baseline Constrained LAMBDA Method for Single Epoch, Single Frequency Attitude Determination Applications. *Proceedings of ION GPS-2007*, pages 2962–2973, 2007.

[9] C Park and P J G Teunissen. A Baseline Constrained LAMBDA Method for Integer Ambiguity Resolution of GNSS Attitude Determination Systems. *Journal of Control, Robotics and Systems (in Korean), 14(6), 587-594*, 2008.

[10] P J Buist. GNSS Kinematic Relative Positioning for Spacecraft: Data Analysis of a Dynamic Testbed. *26th ISTS (International Symposium on Space Technology and Science, Hamamatsu, Japan, 1-8 June 2008*, 2008.

[11] P J Buist, P J G Teunissen, G Giorgi, and S Verhagen. Instantaneous Multi-Baseline Ambiguity Resolution with Constraints. *International Symposium on GPS/GNSS 2008, Tokyo, Japan, 11-14 November 2008*, 2008.

[12] P J Buist, P J G Teunissen, G Giorgi, and S Verhagen. Multi-Platform Instantaneous GNSS Ambiguity Resolution for Triple and Quadruple Antenna Configurations with Constraints. *International Journal of Navigation and Observation*, 2009.

[13] P J G Teunissen. A General Multivariate Formulation of the Multi-Antenna GNSS Attitude Determination Problem. *Artificial Satellites*, 42(2):97–111, 2007.

[14] P J Buist, S Kumagai, T Ito, K Hama, and K Mitani. Development of the Integrated Navigation Unit; Combining a GPS Receiver with Star Sensor Measurements. *Proceedings of the 10th International Conference of Pacific Basin Societies (ISCOPS)*, 2003.

[15] S Verhagen. Visualization of GNSS-related design parameters: Manual for the Matlab user interface VISUAL. 2006.

[16] M O Kechine, C C J M Tiberius, and H van der Marel. Experimental Verification of Internet-based Global Differential GPS. *Proceedings of ION-GPS/GNSS-2003*, pages 28–37, 2003.

[17] P J G Teunissen. Success probability of integer GPS ambiguity rounding and bootstrapping. *Journal of Geodesy*, 72:606–612, 1998.

[18] G Giorgi and P J Buist. Single-Epoch, Single-Frequency, Standalone Full Attitude Determination: Experimental Results. *Proceedings of NAVITEC, Noordwijk, The Netherlands, 10-12 December 2008*, 2008.